remote sensing

MDPI

Article

Land-Use and Land-Cover Changes in Cottbus City and Spree-Neisse District, Germany, in the Last Two Decades: A Study Using Remote Sensing Data and Google Earth Engine

Rezwan Ahmed [1,*], Md. Abu Zafor [2] and Katja Trachte [1]

[1] Department of Atmospheric Processes, Brandenburg University of Technology Cottbus-Senftenberg, 03046 Cottbus, Germany; katja.trachte@b-tu.de
[2] Department of Civil Engineering, Bangladesh Army International University of Science and Technology (BAIUST), Comilla 3501, Bangladesh; zaforce@baiust.edu.bd
* Correspondence: rezwan.ahmed@b-tu.de; Tel.: +49-0355691105

Abstract: Regular detection of land-use and land-cover (LULC) changes with high accuracy is necessary for natural resources management and sustainable urban planning. The produced LULC maps from Google Earth Engine (GEE) also illustrate the transformation of the LULC for the respective landscape over time. The selected study area, Cottbus City and the Spree-Neisse district in northeastern Germany, has undergone significant development over the past decades due to various factors, including urbanization and industrialization; also, the landscape has been converted in some areas for post-mining activities. Detection of LULC changes that have taken place over the last few decades thus plays a vital role in quantifying the impact of these factors while improving the knowledge of these developments and supporting the city planners or urban management officials before implementing further long-term development initiatives for the future. Therefore, the study aims to (i) detect LULC changes for the time slices 2002 and 2022, testing machine learning (ML) algorithms in supervised and unsupervised classification for Landsat satellite imageries, and (ii) validate the newly produced LULC maps with the available regional database (RDB) from the federal and state statistical offices, Germany, and the Dynamic World (DW) near real-time 10 m global LULC data set powered by artificial intelligence (AI). The results of the Random Forest (RF) and the Smilecart classifiers of supervised classification using Landsat 9 OLI-2/TIRS-2 in 2022 demonstrated a validation accuracy of 88% for both, with Kappa Index (KI) of 83% and 84%, respectively. Moreover, the Training Overall Accuracy (TOA) was 100% for both years. The wekaKMeans cluster of the unsupervised classification also illustrated a similar transformation pattern in the LULC maps. Overall, the produced LULC maps offered an improved representation of the selected region's various land-cover classes (i.e., vegetation, waterbodies, built areas, and bare ground) in the last two decades (20022 to 2022).

Keywords: LULC; machine learning; Landsat; Google Earth Engine; supervised; unsupervised

check for updates

Citation: Ahmed, R.; Zafor, M.A.; Trachte, K. Land-Use and Land-Cover Changes in Cottbus City and Spree-Neisse District, Germany, in the Last Two Decades: A Study Using Remote Sensing Data and Google Earth Engine. *Remote Sens.* **2024**, *16*, 2773. https://doi.org/10.3390/rs16152773

Academic Editor: Dino Ienco

Received: 15 May 2024
Revised: 10 July 2024
Accepted: 27 July 2024
Published: 29 July 2024

Copyright: © 2024 by the authors. Licensee MDPI, Basel, Switzerland. This article is an open access article distributed under the terms and conditions of the Creative Commons Attribution (CC BY) license (https://creativecommons.org/licenses/by/4.0/).

1. Introduction

Changes in land use and land cover (LULC) are affected by human activities and their interaction with nature. Our environment is experiencing this phenomenon due to population growth, deforestation, urbanization, technology, economic development, and lack of proper land use patterns [1]. Ecological landscape functions and processes are also affected by the LULC changes, and a broad understanding of such changes always concerns the landscape ecologist [2]. Since the completion of the German unification in October 1990, the selected study area, Cottbus city and the Spree-Neisse district, has become a regional center in the state of Brandenburg, Germany. Consequently, there have been numerous structural changes and developments in the economy of this region during the last few decades [3]. Therefore, detecting changes in land use as well as in land cover is vital in this region for environmental assessment, natural resource management,

urban and regional planning, and agricultural production management [4]. Furthermore, understanding the relationships between human and natural phenomena is crucial for a better decision-making process, and timely and accurate change detection of the Earth's surface is extremely important.

Numerous techniques have been performed by many researchers to obtain meaningful LULC change information from satellite data [5]. Technologies have been applied to assess environmental change detection and various methodologies, with changeable degrees of resources, outlays, proficiency, and accuracy [6]. Although there is no universal change detection method, it depends on the final user to choose the most appropriate approach by considering the available remote sensing (RS) data, time frame, and study objectives [7,8]. From the change detection analysis, a land-use modeling approach can later comprehend extracted information since the simulation of the LULC is considered valuable for various purposes like environmental impact assessment, land use planning, and policy-making [9,10].

In recent decades, remote sensing data have been broadly used as primary sources for change detection and have significantly impacted urban planning authorities and land-management initiatives [11,12]. The LULC changes information is also essential for numerous studies, including agricultural monitoring and policy making, climate change, urban planning, measuring land and shoreline erosion, wetlands, forestry, and hazard monitoring [13]. Thus, RS became a reliable source of LULC information as the technology offers to obtain and analyze data from ground-based, Earth-orbiting platforms and atmospheric data with linkages to Global Positioning System (GPS) data, emerging modeling accessibilities, and various functions and layers of Geographical Information System (GIS) data [14–16]. Coupled with the availability of historical RS data, the reduced data cost and increased resolution of satellite platforms for observing the LULC with a wide range of spatial scales significantly impact planning agencies and land management initiatives [12]. LULC changes are also essential tools for assessing global change in spatiotemporal scales [17].

In this regard, the GEE Application Programming Interface (API) has been used as a cloud-computing platform for analyzing satellite images, along with machine learning (ML) algorithms to classify LULC changes [18]. GEE can also process big geo data for large areas to observe and predict environmental changes for long periods of time [19,20]. Multi-temporal maps have been developed, including the normalized difference vegetation index (NDVI), and global urban and industrial oil-palm plantations based on Landsat satellite images using ML algorithms on GEE [20–22]. Overall, GEE is a reliable platform for numerous researchers to analyze LULC changes using Landsat satellite imagery [23,24].

Machine Learning classifiers such as Classification and Regression Trees (CARTs), Random Forest (RF), K-Nearest Neighbors (KNN), and the Support Vector Machine (SVM) are also commonly used to provide highly accurate results for LULC classification using Landsat satellite imagery [25–27]. With the advancement in Earth observation technologies, ML techniques have the potential for time-series mapping of LULC on the GEE for large numbers of satellite data [28].

Numerous research studies have been carried out on supervised and unsupervised classification techniques to analyze the Landsat satellite imagery of a selected region for the LULC changes on GEE [29]. Because of the excellent performance, supervised machine learning algorithms, such as Random Forest (RF) and CART classifier, have also been implemented in empirical studies [30]. The ee.Clusterer.wekaKMeans() algorithm is used in unsupervised classification to generate LULC mapping [31].

Recent studies have demonstrated the efficiency of the machine learning algorithms for highly accurate LULC changes with an increased value of overall accuracy (OA) and kappa index (KI) while using Landsat satellite imagery on the GEE platform. For instance, the RF classifier is applied with Landsat satellite imagery 3/5/7/8 to analyze four decades of LULC changes in semi-arid Tunisia on GEE, where the OA was $\geq$96% and the KI was $\geq$93% [32]. Another study conducted in the Northeastern Tibetan Plateau in China to

identify the changes from 2000 to 2018 due to the increased human activities and climate change demonstrated that, despite around 50% of grassland and some major driving forces like elevation and population density, an overall accuracy can be achieved of up to 90%, with kappa values > 86% [33]. The authors of [34] applied an RF approach on GEE to detect the LULC changes from 1986 to 2020. For each year, they have obtained an annual overall classification accuracy ranging from 90% to 95%. Similarly, the authors of [35] classified the LULC in the western and southwestern forest areas of Côte d'Ivoire for 2020 using Landsat 8 Surface Reflectance Tiers 1 Operational Land Imager (OLI)/Thermal Infrared Sensor (TIRS) imagery and Random Forest classifiers on GEE, where they achieved an overall accuracy of over 90%. A land cover (LC) dataset was developed in China from 1993 to 2018 using ML algorithms, where the highest OA was 92.7%, and the LC map was also compared with the Dynamic World, which closely demonstrated the LC type in satellite images [36]. A new approach based on statistical data and the CORINE land cover dataset was applied in Poland and Hungary to analyze LULC changes in 2000 and 2012, which showed a decrease in agricultural areas and an increase in artificial surfaces, forests, and semi-natural regions [37]. Another study in Spain found an increase in forest and shrub land uses in depopulated areas but a decline in agricultural land areas using the CORINE land cover dataset for 2000 and 2018 [38].

Considering the significance of the abovementioned matter and observing a lack of such research in the chosen region (to the best of our knowledge), we initiated this study to achieve an improved LULC map compared to the existing traditional LULC map. Therefore, the objectives of this study are (i) the detection of LULC changes over a 20-year time period (2002 and 2022), testing ML algorithms in supervised and unsupervised classification for Landsat satellite imagery, and (ii) to validate the newly produced LULC maps from the GEE API with the DW near real-time (NRT) global 10 m LULC mapping and regional database (RDB) from the federal and state statistical offices, Germany.

The target area, Cottbus city, and the Spree-Neisse district is a region that is undergoing a major transformation phase. In recent years, the closure of one of the largest open-cast lignite mining sites in eastern Germany (Cottbus Nord) has impacted this region's socioeconomic and environmental conditions, altering ecosystem functions, and the post-mining landscapes [39]. Currently, the Cottbus Nord open-cast mine site is turning into the largest post-mining lake in Germany, namely Cottbuser Ostsee [40]. Thus, the region is acting as a living lab, which makes it highly relevant for analyzing land use and land changes [41].

2. Study Area

The study area covers Cottbus city and the Spree-Neisse district of the Brandenburg state, which are situated in the eastern part of Germany (Figure 1). Cottbus is known as a university city. Around 99,502 people live here in a total land area of 165.0 km^2 (as of 30 June 2023) [42]. An open-cast lignite mine was active in Cottbus Nord until 2015, and it is now turning into the largest post-mining multi-purpose lake in Germany, namely "Cottbuser Ostsee". The economy of the city is based on industries, including construction, fishing, and manufacturing. Spree-Neisse district is formed of some small towns and villages around Cottbus city. The total land area of the district is 1657 km^2, with a population of around 112,493 (as of 31 December 2022) [43]. Spree-Neisse is known as one of the most important industrial areas of the state. Traditionally, the economy of the district lies in the lignite and energy industries. Other industries, including food, chemical, plastic, metal, and building and construction, are also available in this region. The climatic conditions in Cottbus city and Spree-Neisse district are warm and temperate. According to the Köppen–Geiger climate classes, the climate classification in this region is Cfb* [44,45]. The average annual temperature of this region reaches up to 10.4 °C, with a yearly precipitation of around 685 mm. * Temperate Oceanic Climate; C = warm temperature, f = Fully humid, b = warm summer.

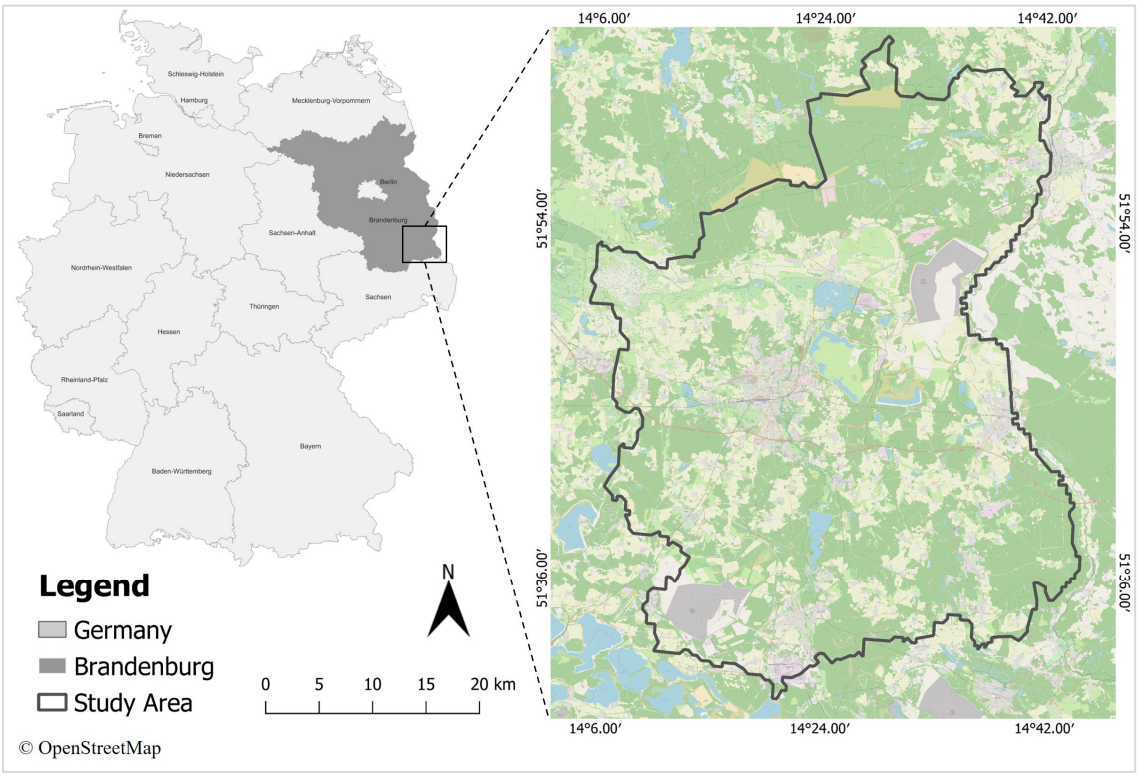

Figure 1. Location of the Study Area in Germany.

3. Data and Methods

3.1. Datasets

3.1.1. Satellite Imagery

To detect the LULC changes in the study area, Landsat 7 and Landsat 9 satellite imagery data were obtained from the United States Geological Survey (USGS) (accessed on October 2023). The details of the Landsat satellite images are presented in Table 1. Collection 2 Tier 1 Top-of-atmosphere (TOA) Reflectance data from Landsat 7 Enhanced Thematic Mapper Plus (ETM+) and Landsat 9 Optimal Land Imager-2 (OLI-2) were used, covering the period from 1 January to 31 December for the years 2002 and 2022. The time slices were selected in order to analyze the major transformation of the living lab over the past years.

Table 1. Details of Landsat imagery used for LULC change detection.

Data Sets	Acquisition Date	Date of Access	Resolution (m)
USGS Landsat 7 Collection 2 Tier 1 TOA Reflectance	1 January 2002 to 31 December 2002	5 December 2023	30
USGS Landsat 9 Collection 2 Tier 1 TOA Reflectance	1 January 2022 to 31 December 2022	5 December 2023	30

All the satellite images were sorted by cloud cover, and only those with minimal cloud cover were selected. The "TrueColor" band combination was applied for each year to detect LULC changes. All relevant datasets were processed using the GEE API.

3.1.2. Training Inputs

A critical step in LULC mapping is selecting training inputs. The GEE Application Programming Interface (API) was used to categorize the total study area based on pixel values, implementing three different ML classifiers: Weka, Smile Cart, and RF. Training

and validation samples were selected through visual inspection of the high-resolution satellite imagery in the GEE. Seventy percent (70%) of the samples were used for training, while the remaining 30% were used for validation. Previous studies indicate that the OA can be achieved at 90% or even more when the training sample size is sufficiently large (i.e., greater than 750 pixels/class) and represents approximately 0.25% of the total study area [46]. Based on the historical evolution of this region over the past few decades [3], we used four land-use classes, summarized in Table 2.

Table 2. Description of LULC classes in the study area.

LULC Type	Description
Water	All the permanent and seasonal water bodies
Vegetation	All the green areas, including agricultural land, forests, parks, etc.
Built Area	Low and high density buildings, roads, and urban open space
Bare ground	Beaches, exposed rocks, sand dunes, quarries, and gravel pits

Additionally, a thorough visual interpretation was conducted using high-spatial-resolution imagery from Google Earth Pro, and regional land-cover types were evaluated using data from the RDB.

3.2. Methodology

To detect LULC changes, we adopted the workflow as presented in Figure 2, utilizing GEE for initial processing and ArcGIS for advanced spatial analysis.

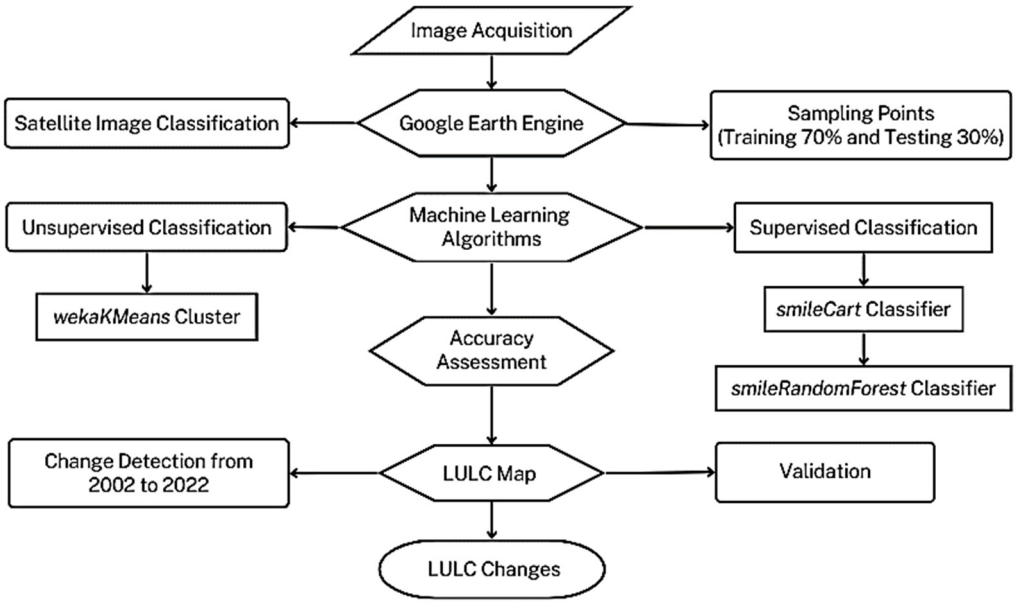

Figure 2. Workflow diagram of the methodology.

3.2.1. Classification

Various ML algorithms and methods are available for detecting LULC changes [47]. However, in this study, ML approaches like unsupervised and supervised classification were performed to analyze the Landsat satellite imagery. For unsupervised classification, we applied the wekaKMeans clustering algorithm to detect LULC changes throughout the study period. This technique is widely used in ML and computational geometry to minimize the average squared distance between points within the same cluster [45,48].

For supervised classification, we employed two different classifiers on the GEE: smileCart (ee.Classifier.smileCart) and RandomForest (ee.Classifier.smileRandomForest). These

classifiers were adopted on GEE for supervised classification. The classification and regression tree (CART) is an efficient regression model that focuses on classification data by constructing a set of rules, requiring no complex domain knowledge [49]. Previous studies showed that RF and CART can produce LULC maps with high accuracy, up to 98% [50]. RF uses a bootstrapped sample (i.e., random sample with replacement), and the features (e.g., spectral bands) are randomly selected to decorrelate the trees, where the splits are determined for varying features [51]. Hence, the RF algorithm can use many trees for the ensemble while handling high-dimensional data [52].

3.2.2. Accuracy Assessment

Accuracy assessment is a crucial part of studying Landsat satellite-imagery classification and the LULC changes over time, enabling more accurate identification of transformations. It is also essential to determine the accuracy of each classification method to ensure the effectiveness of the resulting data for change detection analysis [53]. Three factors should be considered in accuracy assessment: "true" land cover types, intended usage of the classification, and other possible subsets of data within a GIS [54]. Since the collection of ground-truth or reference data to assess the accuracy of the classification results is challenging, the post-classification methods for detecting the changes in LULC largely depend on the accuracy of individual classification results [55]. Many suitable methods exist to assess LULC change detection. In this study, we used the widely accepted method for accuracy assessment, the error-matrix or confusion-matrix method on GEE to determine the Kappa Index (KI) [55]. Several studies demonstrate that KI values ranging from 61% to 80% represent a "Good" or "Acceptable" classification for LULC changes [35].

3.2.3. Validation

In order to estimate uncertainties in the LULC classification, the produced maps from GEE were additionally validated against the real-time data from the Dynamic World (DW). DW is an openly licensed AI-powered NRT 10 m resolution global LULC dataset based on Sentinal-2 Top-of-Atmosphere data generated using deep learning techniques (https://dynamicworld.app/) (accessed on 16 November 2023). For LULC data production, users can add custom rules on GEE to analyze specific classes of interest. The DW taxonomy maintains the land use classes as outlined in the Intergovernmental Panel on Climate Change (IPCC) Good Practice Guidance [56,57]. Many research groups have developed global LULC maps using this dataset, which is considered reliable for quantifying accuracy of the global 10 m LULC products [56,58]. In order to extract data from DW imagery, initially, they were imported on the GEE API and later in ArcGIS 10.8.2 for further analysis of LULC changes. Additionally, the data extracted from the maps were compared with the available regional database (RDB) from the federal and state statistical offices in Germany (www.statistikportal.de, accessed on 16 November 2023) to verify the proportions of different LULC classes. The RDB is generated by statistical surveys while observing mass phenomena, including economic and social.

4. Results

4.1. Unsupervised Classification

Results of the unsupervised classification for the years 2002 and 2022 are displayed in Figures 3 and 4, respectively, highlighting significant changes in the study area. For both years, vegetation covered most of the study area, increasing from 1200 km^2 (69%) in 2002 to 1332 km^2 (76%) in 2022. Consequently, vegetation covers a large amount of the land area in the northern and southern parts of the region. Land cover for both built areas and bare ground has decreased throughout this time. The built area has declined by 100 km^2 within the last two decades and occupies a little more than 250 km^2 now, followed by the bare ground, which is around 8% or 130 km^2 of the total land area. In 2022, water bodies capped the most minimal land area of the region, around 2% or 30 km^2, a little more than in 2002, which was around 27 km^2. Overall, the analysis from the unsupervised classification using

the wekaKMeans cluster illustrated the changes in some significant LULC classes over a period of 20 years.

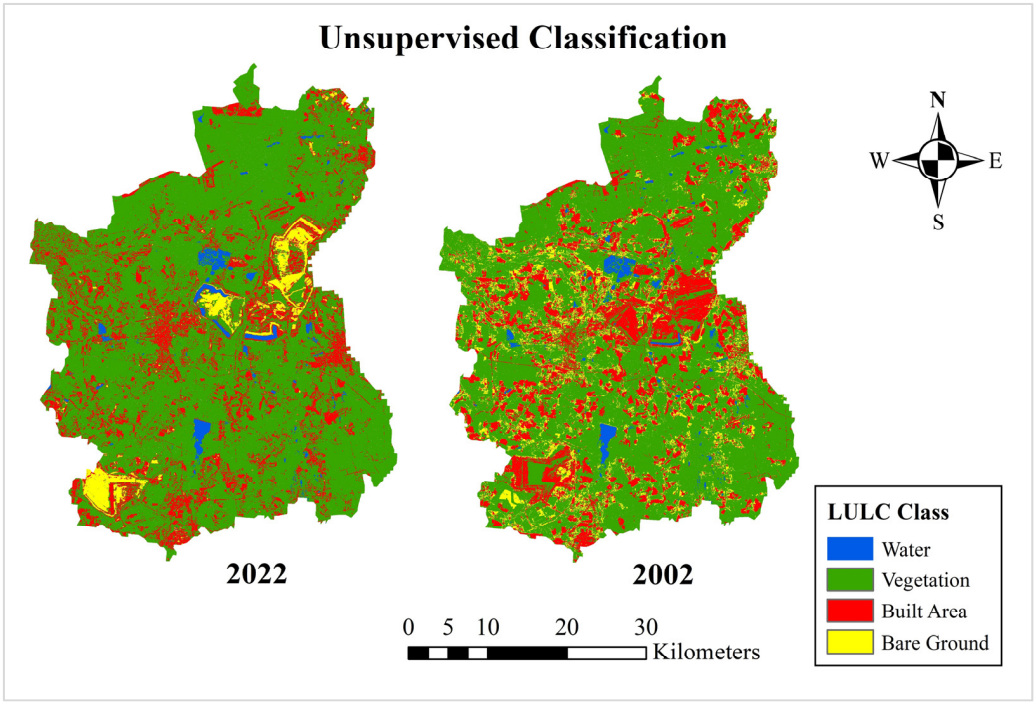

Figure 3. LULC maps of 2002 and 2022 of unsupervised classification.

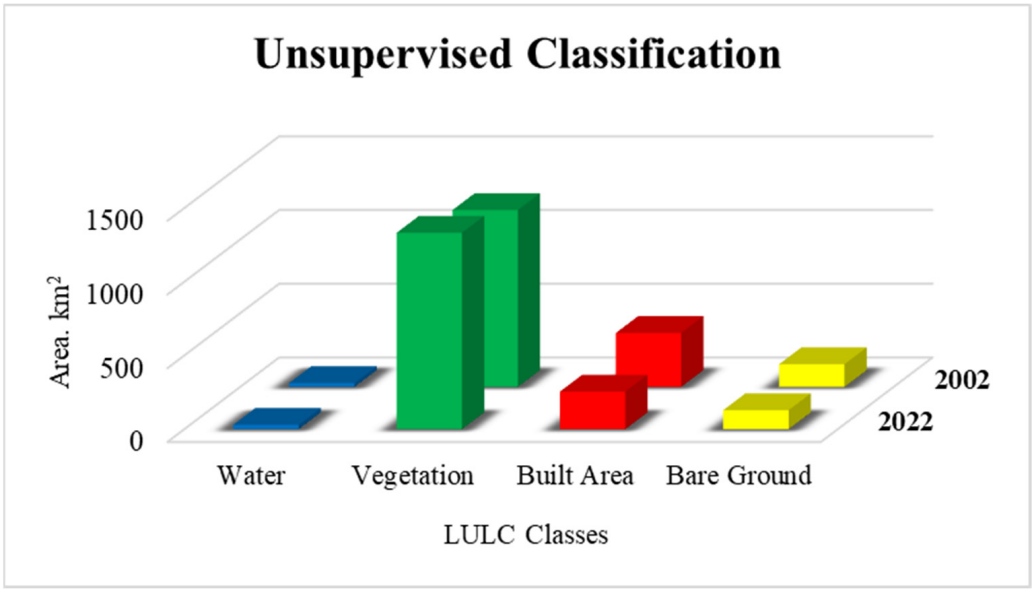

Figure 4. LULC changes for the years 2002 and 2022 (in area, km^2).

4.2. Supervised Classification

4.2.1. SmileCart Classifier

For both of the satellite imageries (Landsat 7 and 9), the supervised classification was conducted in Google Earth Engine using SmileCart classifier while selecting the competent number of training inputs for each of the four land-cover classes. The maps in Figure 5 show that significant changes have occurred in this region throughout the past years. Figure 6 demonstrates that the area of water bodies which occupied one-fourth of the region has declined from 421 km^2 (24%) in 2002 to 150 km^2 (9%) in 2022, followed by the

built area, which has also declined to 171 km^2 or only 10% of the total land area in 2022. The vegetation's land cover was the most during the last two decades, canvasing 28% or 487 km^2 in 2002 to 47% or 815 km^2 in 2022, while bare ground was the next extensive land-cover class, with an area of 610 km^2 or 35% in 2022, which was a little less than 500 km^2 in 2002.

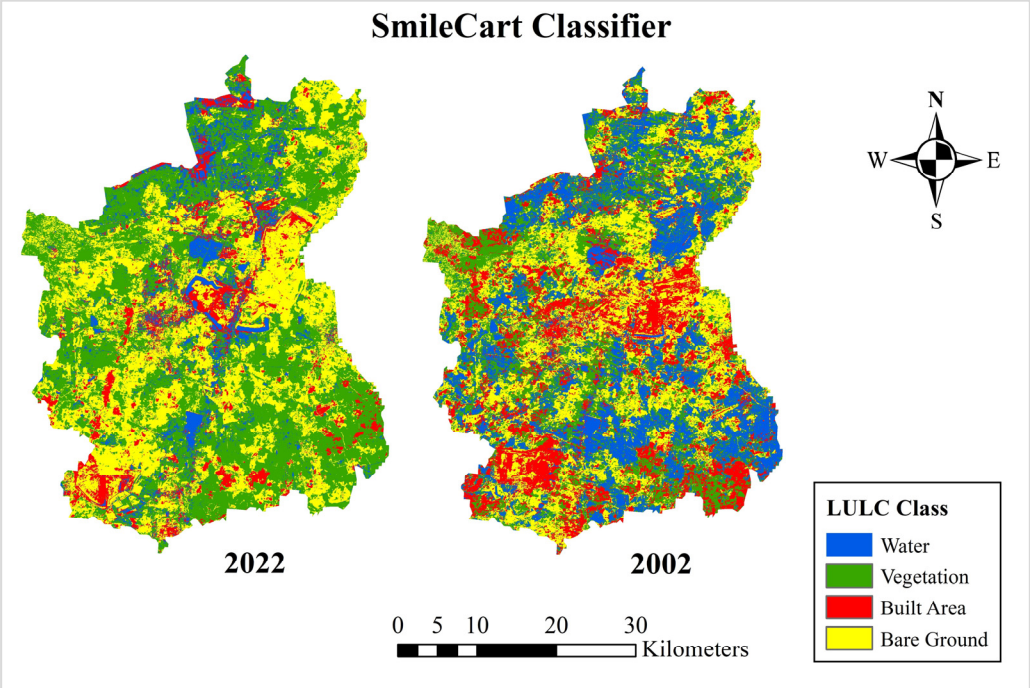

Figure 5. LULC maps of 2002 and 2022 of SmileCart Classifier in supervised classification.

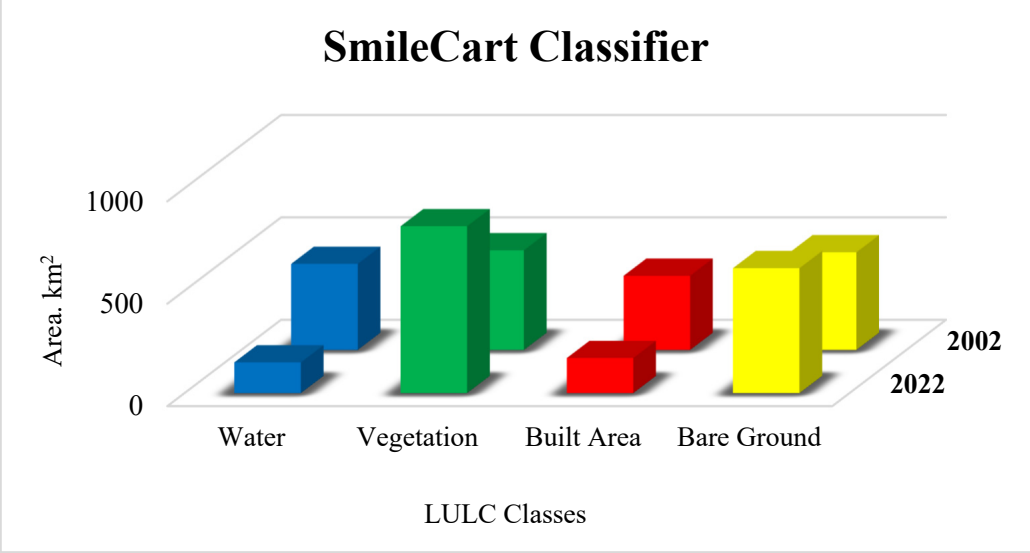

Figure 6. LULC changes for the years 2002 and 2022 (in area, km^2).

4.2.2. SmileRandomForest Classifier

The Random Forest ML algorithm was also applied on the Earth Engine using the SmileRandomForest classifier. Like the SmileCart Classifier, abundant training inputs were taken for each land-cover class; additionally, a suitable number of decision-making trees were considered for the analysis. The changes in the LULC over the past two decades are portrayed on the maps in Figure 7, and also in Figure 8. Like the other two classifiers

from unsupervised and supervised classification, vegetation was also the most expanded land-cover class in 2022, extending to around 983 km^2 or 56% of the land, a little less than in 2002, when it was 1004 km^2 (57%). On the other hand, over the years, the bare ground has increased, and covers an area of 500 km^2 or 29% in 2022, which is almost double that of 2002, 259 km^2 (15%). The area of water land cover has also declined from over 300 km^2 in 2002 to around 150 km^2 or 8% in 2022. Throughout these years, the built area has transformed into other different land uses, hence decreasing to 123 km^2 or 7% in 2022.

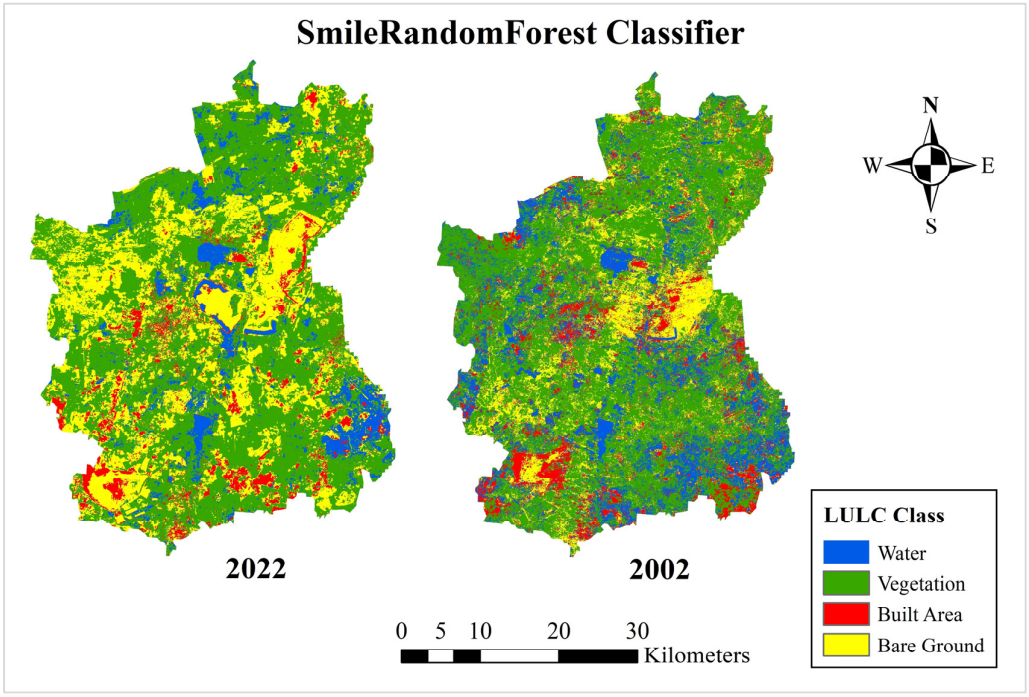

Figure 7. LULC maps of 2002 and 2022 of SmileRandomForest Classifier in supervised classification.

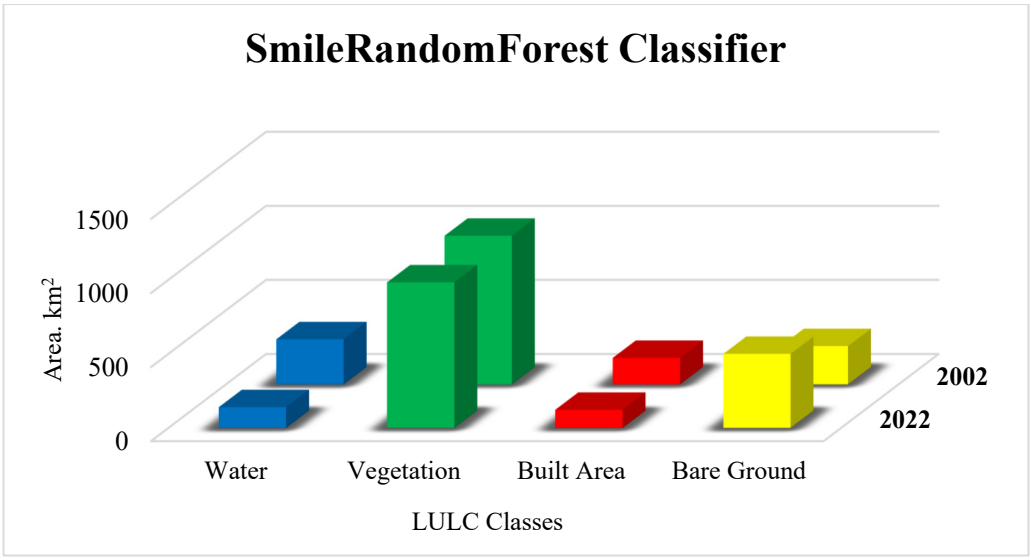

Figure 8. LULC changes for the years 2002 and 2022 (in area, km^2).

4.3. Data Validation

After extracting the data from the LULC maps of 2022 produced in GEE, they were compared with the available database from the DW (the LULC database was available from 27 June 2015) [57], and the RDB from the federal and state statistical offices in Germany

(LULC data for the selected region was available from 31 December 2016) [59]. Figure 9 displays the LULC maps of the study area in 2022 produced from the DW. The data set from DW and RDB illustrated the fact that vegetation was the most extensive land-cover class in 2022, covering an area of 959.44 km^2 (55%) and 1422.82 km^2 (78%), respectively, which is also similar to the results extracted from the LULC maps for the selected classifiers. The land covers of the bare ground (33%) and built area (8%) are the second and third most expansive classes in DW, respectively. However, according to the RDB and DW, throughout this time, water was the region's least-growing land-cover class, covering an area of 56.46 km^2 (3%) and 71.51 km^2 (4%), respectively. Overall, the changes in the land-cover classes in 2022 are similar to the maps produced from unsupervised and supervised satellite image classification in Earth Engine API. An overview of the area of different LULC classes in the selected clusters from the ML algorithms, RDB and DW, is presented in Table 3.

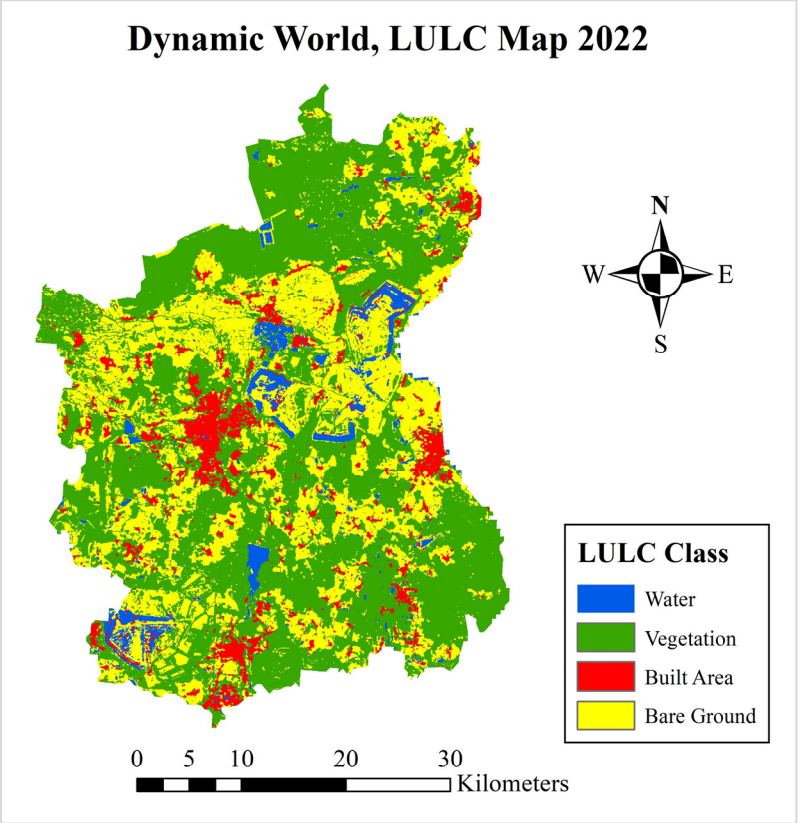

Figure 9. Dynamic World near real-time global 10 m LULC mapping, 2022.

Table 3. Total study area (in km^2) in 2022 according to the selected classifiers, RDB and DW.

LULC Class	wekaKMeans	SmileCart	SmileRandomForest	RDB	DW
Water	29.9	150	141	56.46	71.51
Vegetation	1332.3	815	983	1422.82	959.44
Built Area	254.9	171	123	269.04	139.57
Bare Ground	129.3	610	500	74.28	576.36
Total Area, km^2	1746.4	1746.39	1746.40	1822.6	1746.88

4.4. Classification Performance

Since accuracy assessment is an essential part of detecting the LULC changes more accurately, it was considered for all four maps from supervised ML algorithms. The training

overall accuracy (TOA), validation accuracy (VA), and Kappa Index (KI) were achieved from the Earth Engine to analyze different class performances and misclassifications. Results on the GEE showed that the Random Forest classifier provided TOA $\geq$ 90%, VA $\geq$ 72% (88% in 2022 and 72% in 2002), and KI 83% (2022) and 51% (2002). For the smilecart classifier, the TOA was 100% for all the Landsat satellite images. The KI in 2022 was 84%, and in 2002, it was 66%. The VA for Landsat 7 (2002) was 75%, and for Landsat 9 (2022) it was 88%. Throughout the last 20-year period (2002 to 2022), the way in which the area of the LULC classes of four different categories has changed in the selected study is presented in Table 4.

Table 4. LULC-class area in 2002 and 2022 of the selected classifiers.

Classifier	LULC Class	Area, %		Total Area, km^2	
		2002	2022	2002	2022
wekaKMeans	Water	1.51	1.71	1746.36	1746.4
	Vegetation	68.7	76.29		
	Built Area	20.96	14.6		
	Bare Ground	8.82	7.4		
SmileCart	Water	24.08	8.6	1746.37	1746.39
	Vegetation	27.88	46.66		
	Built Area	20.74	9.8		
	Bare Ground	27.3	34.94		
SmileRandomForest	Water	17.46	8.05	1746.44	1746.40
	Vegetation	57.47	56.28		
	Built Area	10.26	7.02		
	Bare Ground	14.81	28.65		

5. Discussion

Regular LULC change detection provides various types of information on land surface transformation, which is helpful for land use planners and decision-makers with respect to the possible impacts of these environmental changes. In this study, we analyze the land-use and land-cover changes in the last two decades (2002 to 2022) of the selected region by using unsupervised and supervised machine learning algorithms on the Google Earth Engine API. To process the data, ArcMap 10.8.1 was also used.

Despite the implication of different types of Landsat satellite image classifiers in unsupervised and supervised classification, vegetation was the most dominating land-cover type within the study time period, and the aerial coverage has increased over the last few decades. However, uncertainties in the classification can evolve, mainly due to the resemblance of the pixel colors of vegetation and water. This mainly occurs in some parts of the region, especially where trees or forests surround water bodies (e.g., lakes) or where the water's pixel represents a similar pixel color to the trees or forest. This is supposed to be the main reason for having more extensive areas of waterbodies in 2002 (Landsat 7) for both SmiliCart and SmileRandomForest classifiers in supervised image classification. Also, in unsupervised classification, water and vegetation classes overlapped, primarily due to image fusion. Furthermore, the land area of water bodies has declined during the last 20 years due to various factors, including insufficient rainfall and high temperatures, which is one of the main reasons for decreased waterbodies in 2022 [59]. Similarly, due to the decreasing population settlement density in eastern Germany (where the study area is located), land uses have changed over the past year, which clarifies the less-built-up area in 2022 compared to that of 2002 [60]. On the other hand, the area of bare ground has expanded over the last two decades as a result of the massive demolition of the housing and commercial spaces in the many cities of the former GDR (German Democratic Republic), including eastern Germany, after the German reunification [61].

Previous studies also demonstrated that achieving accurate LULC data from high-resolution sensors like Landsat multispectral satellite imagery is challenging over a large area, due to the visual interpretation or satellite image fusion and intense time consump-

tion [62–64]. Despite this, the ranges of the various LULC classes of the produced maps are similar to the real-time statistical data obtained from the RDB and DW (as mentioned in Section 4.4).

Additionally, the confusion matrix or error matrix (4 × 4) on the GEE highlights the misclassification, which has occurred to a smaller extent in all the produced maps in supervisedimage classification, although it is a common phenomenon for LULC change detection, due to the corresponding pixels among deep-water, shallow-water, and vegetated areas [65]. The confusion matrix of the SmileCart classifier in 2022 showed that only one instance (out of four) of both vegetation and built areas was misclassified as bare ground. However, an increased value of TOA (100%) and VA (88.24%) indicated that the map was highly accurate or that most of the classes were True Positive (TP). Similar results were also achieved in the map produced for 2002, where one instance of the confusion matrix (False Negative or FN = 1) of both bare ground and water was misclassified as a built area. The results of the smileRandomForest classifier demonstrated a highly accurate LULC map for 2022 with only one misclassification of a built area, where both the TOA and VA were 100% and 88%, respectively. On the other hand, the results from 2002 using Landsat 7 showed the misclassification of two to three instances of vegetation and built area, which counted as either bare ground or water. However, the 93% TOA represents a relatively high accuracy for most classes. Through various analyses of satellite imagery classifications, many authors have shown more significant evidence that the quality and size of the training samples or sets cause the misclassification, the overlapping of classes, or inaccuracy of total size of the selected study area [66,67].

Furthermore, a possibility for the lower accuracy of the produced LULC maps can be the number of training samples taken on the GEE, although recent studies produced LULC mapping with less than 70% OA [68,69]. However, the KI of supervised classification in 2022 demonstrated the highest accuracy; thus, the produced LULC maps can be used for similar future research [70,71].

According to the RDB, the total land area of the selected region was around 1812 km^2 in 2002, which has increased over the last decades to 1822 km^2 in 2022 [72]. On the other hand, the total area of the selected regions' shape file utilized on Earth Engine and ArcGIS was around 1747 km^2 for both years (2002 and 2022), which was achieved by the European Environment Agency (EEA) [73]. To minimize this divergence, an alternative approach was initially used to draw a group of polygons on the Earth Engine; however, due to the polygon's structural shape, it could not serve the intended purpose very well.

The LULC maps' validation platform, the DW NRT 10 m resolution global LULC dataset, is the world's first NRT product based on deep learning methods. Since, in comparison with the real-time or locally available data, the overall accuracy of DW claimed to be more than 78% accurate for high-resolution (10–30 m) LULC products, and based on previous studies, it can be considered as a reliable platform for map validation [74]. Despite the differences in total area, the proportion of the selected land-cover types of the RDB dataset (second validation platform) was identical to the dataset extracted from the produced LULC maps, especially for the year 2022. On the RDB website, details of LULC survey data were available from 2016 till the end of 2022 for the selected study area (date of data acquisition: 22 November 2023). Also, the RDB is chosen over other satellite imagery sources for validation data because they had to be processed either on GEE or ArcGIS to achieve the data set for the selected region.

It is also worth noting that the validation accuracy varies based on various factors, including the Landsat satellite imagery, percentage (%) of cloud cover of the satellite imagery, type and quantity of land-cover classes, number of decision-making trees in RF classification, region of study, and the selected time period. Since the Landsat satellite imagery completes an orbit every 16 days after crossing every point on Earth, the VA changes from time to time for every region, even for the same training samples [75]. Also, depending on the location, the DW offers global land-cover updates every 2 to 5 days [76].

6. Conclusions

This research aimed to utilize Landsat satellite data and advanced classification methods to detect LULC changes in the Cottbus city and Spree-Neisse district of eastern Germany, providing valuable insights for regional planning and environmental sustainability. It was also essential to monitor the LULC changes over the long-term period for the sustainable management of land and natural resources, especially while considering adopting long-term initiatives to make the selected region a model city for climate protection, sustainability, and financial growth [77]. The combination of unsupervised and supervised classification methods in GEE API testing ML algorithms using USGS Landsat Satellite 7 and 9 imageries proved effective in providing a detailed and reliable understanding of the LULC changes that have taken place over a period of 20 years. After careful visual inspection, we categorized the LULC of the selected region into four distinct classes. The study found significant increases in vegetation cover from 69% to 76% and decreases in built area and bare ground, which indicates positive environmental changes, possibly influenced by regional policies and socio-economic transformation. Validation with multiple platforms like DW and RDB also revealed a similar shift for LULC changes in this region. Also, the higher values of VA and KI indicated high accuracy of the produced maps from the GEE. The clusters of the ML algorithms implemented in the analysis, i.e., wekaKMeans, SmiliCart, and SmileRandomForest, are convincing evidence that these are effective in terms of detecting LULC changes.

These findings have important implications for regional planning and policy-making, particularly in the context of urbanization, post-mining land reclamation, and environmental sustainability. Future research should emphasize a continuous observation of these changes and assess the impact of specific policies and interventions. Future research could focus on integrating higher-resolution satellite data and exploring the socio-economic impacts of LULC changes on local communities. Additionally, examining the role of specific environmental policies in driving these changes could provide valuable insights for other regions undergoing similar transitions.

Continuous monitoring of LULC changes and integration of multi-source data will be crucial in understanding the dynamic interactions between human activities and environmental changes, ensuring sustainable development in this region.

Author Contributions: Conceptualization, R.A.; methodology, R.A.; software, R.A. and M.A.Z.; validation, R.A.; formal analysis, R.A.; investigation, R.A.; resources, R.A.; data curation, R.A.; writing—original draft preparation, R.A.; writing—review and editing, R.A., M.A.Z. and K.T.; visualization, R.A.; supervision, M.A.Z. and K.T. All authors have read and agreed to the published version of the manuscript.

Funding: This research received no external funding.

Data Availability Statement: The data supporting reported results can be achieved from the corresponding author on request.

Conflicts of Interest: The authors declare no conflict of interest.

References

1. Hossain, F.; Moniruzzaman, M. Environmental change detection through remote sensing technique: A study of Rohingya refugee camp area (Ukhia and Teknaf sub-district), Cox's Bazar, Bangladesh. *Environ. Chall.* **2021**, *2*, 100024. [CrossRef]
2. Hietel, E.; Waldhardt, R.; Otte, A. Analysing land-cover changes in relation to environmental variables in Hesse, Germany. *Landsc. Ecol.* **2004**, *19*, 473–489. [CrossRef]
3. Stadt Cottbus: From the History of the City of Cottbus. Available online: https://www.cottbus.de/wissenswert/geschichte/ (accessed on 26 July 2023).
4. Wang, J.; Bretz, M.; Dewan, M.A.A.; Delavar, M.A. Machine learning in modelling land-use and land cover-change (LULCC): Current status, challenges and prospects. *Sci. Total Environ.* **2022**, *822*, 153559. [CrossRef]
5. Tanmoy Das: Land Use/Land Cover Change Detection: An Object Oriented Approach, Münster, Germany. 2009. Available online: https://run.unl.pt/handle/10362/2532 (accessed on 31 July 2023).

6. Mehedy Hassan, M.; Culver Smith, A.; Walker, K.; Khaledur Rahman, M.; Southworth, J. Rohingya Refugee Crisis and Forest Cover Change in Teknaf, Bangladesh. *Remote Sens.* **2018**, *10*, 689. [CrossRef]
7. Kotaridis, I.; Lazaridou, M. Environmental change detection study in the wider area of lignite mines. Civil Engineering and Architecture. *Civ. Eng. Arch.* **2018**, *6*, 103–114. [CrossRef]
8. Tewkesbury, A.P.; Comber, A.J.; Tate, N.J.; Lamb, A.; Fisher, P.F. A critical synthesis of remotely sensed optical image change detection techniques. *Remote Sens. Environ.* **2015**, *160*, 1–14. [CrossRef]
9. Kline, J.D.; Moses, A.; Lettman, G.J.; Azuma, D.L. Modeling forest and range land development in rural locations, with examples from eastern Oregon. *Landsc. Urban Plan.* **2007**, *80*, 320–332. [CrossRef]
10. Schulp, C.J.E.; Nabuurs, G.J.; Verburg, P.H. Future carbon sequestration in Europe—Effects of land use change. *Agric. Ecosyst. Environ.* **2008**, *127*, 251–264. [CrossRef]
11. Lu, D.; Mausel, P.; Brondízio, E.; Moran, E. Change detection techniques. *Int. J. Remote. Sens.* **2004**, *25*, 2365–2401. [CrossRef]
12. Rogan, J.; Chen, D.M. Remote sensing technology for mapping and monitoring land-cover and land-use change. *Prog. Plann.* **2004**, *61*, 301–325. [CrossRef]
13. Prasad, P.; Loveson, V.J.; Chandra, P.; Kotha, M. Evaluation and comparison of the earth observing sensors in land cover/land use studies using machine learning algorithms. *Ecol. Inform.* **2022**, *68*, 101522. [CrossRef]
14. Alshari, E.A.; Gawali, B.W. Development of classification system for LULC using remote sensing and GIS. *Glob. Transit. Proc.* **2021**, *2*, 8–17. [CrossRef]
15. Chughtai, A.H.; Abbasi, H.; Karas, I.R. A review on change detection method and accuracy assessment for land use land cover. *Remote Sens. Appl.* **2021**, *22*, 100482. [CrossRef]
16. Feng, D.D.; Herman, B.M. Remotely Sensing the Earth's Atmosphere Using the Global Positioning System (GPS)—The GPS/MET Data Analysis. *J. Atmos. Ocean. Technol.* **1999**, *16*, 989–1002. [CrossRef]
17. Lambin, E.F. Modelling and monitoring land-cover change processes in tropical regions. *Prog. Phys. Geogr. Earth Environ.* **1997**, *21*, 375–393. [CrossRef]
18. Tassi, A.; Vizzari, M. Object-Oriented LULC Classification in Google Earth Engine Combining SNIC, GLCM, and Machine Learning Algorithms. *Remote Sens.* **2020**, *12*, 3776. [CrossRef]
19. Amani, M.; Ghorbanian, A.; Ahmadi, S.A.; Kakooei, M.; Moghimi, A.; Mirmazloumi, S.M.; Moghaddam, S.H.A.; Mahdavi, S.; Ghahremanloo, M.; Parsian, S.; et al. Google Earth Engine Cloud Computing Platform for Remote Sensing Big Data Applications: A Comprehensive Review. *IEEE J. Sel. Top. Appl. Earth Obs. Remote. Sens.* **2020**, *13*, 5326–5350. [CrossRef]
20. Floreano, I.X.; de Moraes, L.A.F. Land use/land cover (LULC) analysis (2009–2019) with Google Earth Engine and 2030 prediction using Markov-CA in the Rondônia State, Brazil. *Environ. Monit. Assess.* **2021**, *193*, 239. [CrossRef]
21. Liu, X.; Hu, G.; Chen, Y.; Li, X.; Xu, X.; Li, S.; Pei, F.; Wang, S. High-resolution multi-temporal mapping of global urban land using Landsat images based on the Google Earth Engine Platform. *Remote Sens. Environ.* **2018**, *209*, 227–239. [CrossRef]
22. Lee, J.S.H.; Wich, S.; Widayati, A.; Koh, L.P. Detecting industrial oil palm plantations on Landsat images with Google Earth Engine. *Remote. Sens. Appl.* **2016**, *4*, 219–224. [CrossRef]
23. Becker, W.R.; Ló, T.B.; Johann, J.A.; Mercante, E. Statistical features for land use and land cover classification in Google Earth Engine. *Remote. Sens. Appl.* **2021**, *21*, 100459. [CrossRef]
24. Lin, L.; Hao, Z.; Post, C.J.; Mikhailova, E.A.; Yu, K.; Yang, L.; Liu, J. Monitoring Land Cover Change on a Rapidly Urbanizing Island Using Google Earth Engine. *Appl. Sci.* **2020**, *10*, 7336. [CrossRef]
25. Foody, G.M.; Mathur, A. A relative evaluation of multiclass image classification by support vector machines. *IEEE Trans. Geosci. Remote Sens.* **2004**, *42*, 1335–1343. [CrossRef]
26. Nery, T.; Sadler, R.; Solis-Aulestia, M.; White, B.; Polyakov, M.; Chalak, M. Comparing supervised algorithms in Land Use and Land Cover classification of a Landsat time-series. In Proceedings of the 2016 IEEE International Geoscience and Remote Sensing Symposium (IGARSS), Beijing, China, 10–15 July 2016; pp. 5165–5168. [CrossRef]
27. Shiraishi, T.; Motohka, T.; Thapa, R.B.; Watanabe, M.; Shimada, M. Comparative assessment of supervised classifiers for land use-land cover classification in a tropical region using time-series PALSAR mosaic data. *IEEE J. Sel. Top. Appl. Earth Obs. Remote. Sens.* **2014**, *7*, 1186–1199. [CrossRef]
28. Feizizadeh, B.; Omarzadeh, D.; Kazemi Garajeh, M.; Lakes, T.; Blaschke, T. Machine learning data-driven approaches for land use/cover mapping and trend analysis using Google Earth Engine. *J. Environ. Plan. Manag.* **2023**, *66*, 665–697. [CrossRef]
29. Zaidi, S.M.; Akbari, A.; Samah, A.A.; Kong, N.S.; Isabella, J.; Gisen, A. Introduction Landsat-5 Time Series Analysis for Land Use/Land Cover Change Detection Using NDVI and Semi-Supervised Classification Techniques. *J. Environ. Stud.* **2017**, *26*, 2833–2840. [CrossRef]
30. Caruana, R.; Niculescu-Mizil, A. An empirical comparison of supervised learning algorithms. *ACM Int. Conf. Proceeding Ser.* **2006**, *148*, 161–168. [CrossRef]
31. Pierre Pott, L.; Jorge Carneiro Amado, T.; Augusto Schwalbert, R.; Mateus Corassa, G.; Antonio Ciampitti, I. Crop type classification in Southern Brazil: Integrating remote sensing, crop modeling and machine learning. *Comput. Electron. Agric.* **2022**, *201*, 107320. [CrossRef]
32. Kadri, N.; Jebari, S.; Augusseau, X.; Mahdhi, N.; Lestrelin, G.; Berndtsson, R. Analysis of Four Decades of Land Use and Land Cover Change in Semiarid Tunisia Using Google Earth Engine. *Remote Sens.* **2023**, *15*, 3257. [CrossRef]

33. Liu, C.; Li, W.; Zhu, G.; Zhou, H.; Yan, H.; Xue, P. Land Use/Land Cover Changes and Their Driving Factors in the Northeastern Tibetan Plateau Based on Geographical Detectors and Google Earth Engine: A Case Study in Gannan Prefecture. *Remote Sens.* **2020**, *12*, 3139. [CrossRef]
34. Dubertret, F.; Le Tourneau, F.-M.; Villarreal, M.L.; Norman, L.M. Monitoring Annual Land Use/Land Cover Change in the Tucson Metropolitan Area with Google Earth Engine (1986–2020). *Remote Sens.* **2022**, *14*, 2127. [CrossRef]
35. Kouassi, C.J.A.; Qian, C.; Khan, D.; Achille, L.S.; Kebin, Z.; Omifolaji, J.K.; Yang, X. Google Earth Engine for Landsat Image Processing and Assessing Lulc Classification in Southwestern Côte D'ivoire. *Geod. Cartogr.* **2023**, *49*, 37–50. [CrossRef]
36. Naboureh, A.; Li, A.; Bian, J.; Lei, G.; Nan, X. Land cover dataset of the China Central-Asia West-Asia Economic Corridor from 1993 to 2018. *Sci. Data* **2023**, *10*, 728. [CrossRef]
37. Cegielska, K.; Noszczyk, T.; Kukulska, A.; Szylar, M.; Hernik, J.; Dixon-Gough, R.; Jombach, S.; Valánszki, I.; Filepné Kovács, K. Land use and land cover changes in post-socialist countries: Some observations from Hungary and Poland. *Land Use Policy* **2018**, *78*, 1–18. [CrossRef]
38. Gallardo, M.; Fernández-Portela, J.; Cocero, D.; Vilar, L. Land Use and Land Cover Changes in Depopulated Areas of Mediterranean Europe: A Case Study in Two Inland Provinces of Spain. *Land* **2023**, *12*, 1967. [CrossRef]
39. Gerwin, W.; Raab, T.; Birkhofer, K.; Hinz, C.; Letmathe, P.; Leuchner, M.; Roß-Nickoll, M.; Rüde, T.; Trachte, K.; Wätzold, F.; et al. Perspectives of lignite post-mining landscapes under changing environmental conditions: What can we learn from a comparison between the Rhenish and Lusatian region in Germany? *Environ. Sci. Eur.* **2023**, *35*, 36. [CrossRef]
40. On the Way to the Cottbus Baltic Sea. Available online: https://www.leag.de/de/geschaeftsfelder/bergbau/cottbuser-ostsee/ (accessed on 14 August 2023).
41. Hossain, M.; Leminen, S.; Westerlund, M. A systematic review of living lab literature. *J. Clean Prod.* **2019**, *213*, 976–988. [CrossRef]
42. City Administration: Population in Cottbus. Available online: https://www.cottbus.de/aktuelles/statistik/bevoelkerung.html (accessed on 14 August 2023).
43. District Administrator: Population in the Spree-Neisse District. Available online: https://www.lkspn.de/buergerservice/statistik/bevoelkerunglandkreis.html (accessed on 14 August 2023).
44. Climate Data: Data and Graphs on the Climate and Weather in Cottbus. Available online: https://de.climate-data.org/europa/deutschland/brandenburg/cottbus-6314/ (accessed on 14 August 2023).
45. Climate Data: Data and Graphs on the Climate and Weather in Fürstenwalde/Spree. Available online: https://de.climate-data.org/europa/deutschland/brandenburg/fuerstenwalde-spree-22837/ (accessed on 14 August 2023).
46. Noi, P.T.; Kappas, M. Comparison of Random Forest, k-Nearest Neighbor, and Support Vector Machine Classifiers for Land Cover Classification Using Sentinel-2 Imagery. *Sensors* **2017**, *18*, 18. [CrossRef]
47. Richards, J.A. *Remote Sensing Digital Image Analysis*; Springer: Cham, Switzerland, 2022; pp. 1–567. [CrossRef]
48. Arthur, D.; Vassilvitskii, S. k-Means++: The Advantages of Careful Seeding. In Proceedings of the Eighteenth Annual ACM-SIAM Symposium on Discrete Algorithms, New Orleans, LA, USA, 7–9 January 2007; pp. 1027–1035.
49. Cui, Y.; Yang, G.; Zhou, Y.; Zhao, C.; Pan, Y.; Sun, Q.; Gu, X. AGTML: A novel approach to land cover classification by integrating automatic generation of training samples and machine learning algorithms on Google Earth Engine. *Ecol. Indic.* **2023**, *154*, 110904. [CrossRef]
50. Ouma, Y.; Nkwae, B.; Moalafhi, D.; Odirile, P.; Parida, B.; Anderson, G.; Qi, J. Comparison of Machine Learning Classifiers for Multitemporal and Multisensor Mapping of Urban Lulc Features. *Int. Arch. Photogramm. Remote Sens. Spat. Inf. Sci.* **2022**, *XLIII-B3-2022*, 681–689. [CrossRef]
51. Breiman, L. Random Forests. *Mach. Learn.* **2001**, *45*, 5–32. [CrossRef]
52. Gislason, P.O.; Benediktsson, J.A.; Sveinsson, J.R. Random Forests for land cover classification. *Pattern Recognit. Lett.* **2006**, *27*, 294–300. [CrossRef]
53. Owojori, A.; Xie, H. Landsat image-based LULC changes of San Antonio, Texas using advanced atmospheric correction and object-oriented image analysis approaches. In Proceedings of the 5th International Symposium on Remote Sensing of Urban Areas, Tempe, AZ, USA, 14–16 March 2005.
54. Lillesand, T.; Kiefer, R.; Chipman, J. *Remote Sensing and Image Interpretation*; John Wiley & Sons: Hobokan, NJ, USA, 2015.
55. Foody, G.M. Status of land cover classification accuracy assessment. *Remote Sens. Environ.* **2002**, *80*, 185–201. [CrossRef]
56. Brown, C.F.; Brumby, S.P.; Guzder-Williams, B.; Birch, T.; Hyde, S.B.; Mazzariello, J.; Czerwinski, W.; Pasquarella, V.J.; Haertel, R.; Ilyushchenko, S.; et al. Dynamic World, Near real-time global 10 m land use land cover mapping. *Sci. Data* **2022**, *9*, 251. [CrossRef]
57. Penman, J.; Gytarsky, M.; Hiraishi, T.; Krug, T.; Kruger, D.; Pipatti, R.; Buendia, L.; Miwa, K.; Ngara, T.; Tanabe, K.; et al. *Intergovernmental Panel on Climate Change Good Practice Guidance for Land Use, Land-Use Change and Forestry*; IPCC National Greenhouse Gas Inventories Programme; Institute for Global Environmental Strategies (IGES): Kanagawa, Japan.
58. Venter, Z.S.; Barton, D.N.; Chakraborty, T.; Simensen, T.; Singh, G. Global 10 m Land Use Land Cover Datasets: A Comparison of Dynamic World, World Cover and Esri Land Cover. *Remote Sens.* **2022**, *14*, 4101. [CrossRef]
59. The District Administrator: Information on the Current Low Water Situation and Appeal for Economical Use of Drinking, Ground and Surface Water. Available online: https://www.lkspn.de/aktuelles/aktuelles-landkreis-spree-neisse/pressearchiv/44818-information-zur-aktuellen-niedrigwassersituation-und-appell-zur-sparsamen-benutzung-von-trink-grund-und-oberflachenwasser.html (accessed on 10 October 2023).
60. Kroll, F.; Haase, D. Does demographic change affect land use patterns? *Land Use Policy* **2010**, *27*, 726–737. [CrossRef]

61. Schetke, S.; Haase, D. Multi-criteria assessment of socio-environmental aspects in shrinking cities. Experiences from eastern Germany. *Environ. Impact Assess. Rev.* **2008**, *28*, 483–503. [CrossRef]
62. Phinzi, K.; Ngetar, N.S.; Pham, Q.B.; Chakilu, G.G.; Szabó, S. Understanding the role of training sample size in the uncertainty of high-resolution LULC mapping using random forest. *Earth Sci. Inform.* **2023**, *16*, 3667–3677. [CrossRef]
63. Padmanaban, R.; Bhowmik, A.K.; Cabral, P. Satellite image fusion to detect changing surface permeability and emerging urban heat islands in a fast-growing city. *PLoS ONE* **2019**, *14*, e0208949. [CrossRef] [PubMed]
64. Nagel, P.; Yuan, F. High-resolution Land Cover and Impervious Surface Classifications in the Twin Cities Metropolitan Area with NAIP Imagery. *Photogramm. Eng. Remote. Sens.* **2015**, *82*, 63–71. [CrossRef]
65. Amani, M.; Mahdavi, S.; Kakooei, M.; Ghorbanian, A.; Brisco, B.; Delancey, E.; Toure, S.; Reyes, E.L. Wetland Change Analysis in Alberta, Canada Using Four Decades of Landsat Imagery. *IEEE J. Sel. Top. Appl. Earth Obs. Remote. Sens.* **2021**, *14*, 10314–10335. [CrossRef]
66. Mellor, A.; Boukir, S.; Haywood, A.; Jones, S. Exploring issues of training data imbalance and mislabelling on random forest performance for large area land cover classification using the ensemble margin. *ISPRS J. Photogramm. Remote Sens.* **2015**, *105*, 155–168. [CrossRef]
67. Foody, G.M.; Mathur, A.; Sanchez-Hernandez, C.; Boyd, D.S. Training set size requirements for the classification of a specific class. *Remote. Sens. Environ.* **2006**, *104*, 1–14. [CrossRef]
68. Ai, B.; Huang, K.; Zhao, J.; Sun, S.; Jian, Z.; Liu, X. Comparison of Classification Algorithms for Detecting Typical Coastal Reclamation in Guangdong Province with Landsat 8 and Sentinel 2 Images. *Remote Sens.* **2022**, *14*, 385. [CrossRef]
69. Shimizu, K.; Murakami, W.; Furuichi, T.; Estoque, R.C. Mapping Land Use/Land Cover Changes and Forest Disturbances in Vietnam Using a Landsat Temporal Segmentation Algorithm. *Remote Sens.* **2023**, *15*, 851. [CrossRef]
70. Rwanga, S.S.; Ndambuki, J.M. Accuracy Assessment of Land Use/Land Cover Classification Using Remote Sensing and GIS. *Int. J. Geosci.* **2017**, *08*, 611–622. [CrossRef]
71. Talukdar, S.; Singha, P.; Mahato, S.; Shahfahad Pal, S.; Liou, Y.A.; Rahman, A. Land-Use Land-Cover Classification by Machine Learning Classifiers for Satellite Observations—A Review. *Remote Sens.* **2020**, *12*, 1135. [CrossRef]
72. Federal and State Statistical Offices: Regional Database Germany. Available online: https://www.regionalstatistik.de/genesis/online?operation=previous&levelindex=&step=&titel=&levelid=&acceptscookies=false (accessed on 10 October 2023).
73. European Environment Agency: Germany Administrative Boundaries. Available online: https://www.eea.europa.eu/data-and-maps/data/external/germany-administrative-boundaries (accessed on 12 June 2023).
74. Wang, Y.; Sun, Y.; Cao, X.; Wang, Y.; Zhang, W.; Cheng, X. A review of regional and Global scale Land Use/Land Cover (LULC) mapping products generated from satellite remote sensing. *ISPRS J. Photogramm. Remote Sens.* **2023**, *206*, 311–334. [CrossRef]
75. What Are the Acquisition Schedules for the Landsat Satellites? | U.S. Geological Survey. Available online: https://www.usgs.gov/faqs/what-are-acquisition-schedules-landsat-satellites (accessed on 15 June 2023).
76. Dynamic World—10 m Global Land Cover Dataset in Google Earth Engine. Available online: https://dynamicworld.app/about (accessed on 15 June 2023).
77. The Boomtown—BOOMTOWN COTTBUS. Available online: https://www.boomtown.de/die-boomtown.html (accessed on 24 November 2023).

Disclaimer/Publisher's Note: The statements, opinions and data contained in all publications are solely those of the individual author(s) and contributor(s) and not of MDPI and/or the editor(s). MDPI and/or the editor(s) disclaim responsibility for any injury to people or property resulting from any ideas, methods, instructions or products referred to in the content.